Applied Water Science (2024) 14:218
https://doi.org/10.1007/s13201-024-02271-7

ORIGINAL ARTICLE

Eco-friendly synthesis of reduced graphene oxide/palladium composite and its catalytic, antibacterial and antifungal activities for bone regeneration and fracture treatment

Ke Zhang[2] · Shenyi Lu[3] · Mingyang Jiang[2] · Ying Liu[1] · Ruqiong Wei[1]

Received: 1 May 2024 / Accepted: 4 August 2024

Abstract

Nanocomposites based on inorganic/graphene nanoparticles have gained remarkable interest as a novel class of hybrid materials. Scientific community attention towards these substances has been increasing, because of their peculiar characteristics in combining anticipated features of building constructs for specified applications. Graphene oxide (GO) and metal nanoparticles (MNPs) are using separately in different applications due to their specific limitations. Researchers continue to explore ways to overcome these challenges and create functional nanomaterials for various fields by combining unique advantages of GO and MNPs. Here, we used a facile one-step method for the synthesis of reduced graphene oxide–palladium composite (RGO/Pd). Environmental-friendly biofabricated palladium nanoparticles adhered to *Polyscias scutellaria* (PS) leaf extract mediated RGO/Pd have been presented in the current investigation. The biofabricated nanohybrid (RGO/Pd) was analysed utilizing several microscopic and spectroscopic techniques. Further, we have also examined the catalytic function for the reduction of 2-nitroaniline (2-NA) in detail. Primarily, we observed that the synthesized nanocomposite can catalyse simultaneous reduction of 2-NA. Furthermore, an added advantage of the as prepared RGO/Pd nanocomposite is its antimicrobial and antifungal ability. Further, we exhibited that the mesenchymal stem cells of adult goat were viable in the presence of RGO/Pd of 0.1 mg/mL concentration and their properties of stem cells were retained. The outcomes displayed that the nanocomposites exhibited outstanding functioning in the killing of dangerous microbial and fungal pathogens. All these results strengthen the RGO/Pd composite applicability in future for potential therapy in bone tissue engineering applications.

Keywords Graphene · Pd NPs · Antibacterial · Catalytic · Antifungal · Bone regeneration · RGO/Pd

Introduction

Graphene oxide and metal nanoparticles are using separately in different applications due to some limitations like agglomeration (Jana et al. 2017), reduced electrical conductivity, limited mechanical strength (Parnianchi et al. 2018), aggregation, stability, toxicity (Radulescu et al. 2023) and

Ke Zhang, Shenyi Lu and Mingyang Jiang have contributed equally for this work.

✉ Ruqiong Wei
weiruqiongxibanya@163.com

Ke Zhang
kz18202282801@163.com

Shenyi Lu
drlushenyi@163.com

Mingyang Jiang
775873872@qq.com

Ying Liu
yeziming1620@163.com

[1] Department of Rehabilitation Medicine, The First Affiliated Hospital of Guangxi Medical University, No. 6 Shuangyong Road, Qingxiu, Nanning 530021, Guangxi, China

[2] Department of Bone and Joint Surgery, The First Affiliated Hospital of Guangxi Medical University, Nanning 530021, China

[3] Department of Rehabilitation Medicine, The Affiliated Hospital of Youjiang Medical University for Nationalities, Baise 533000, China

Published online: 14 September 2024

size control (Scroccorello et al. 2023). Both GO and MNPs offer unique advantages; thus, researchers continue to explore ways to overcome limitations and create functional nanomaterials for various fields (Ban et al. 2023; Rasuli et al. 2015). Nanocomposites based on inorganic/graphene nanoparticles have gained remarkable interest as a novel class of hybrid materials (Fioravanti et al. 2023; Hashtroudi et al. 2021). Scientific community attention towards these substances has been increasing, because of their peculiar characteristics in combining anticipated features of building constructs for specified applications (Li. et al. 2015). Unique opto-electronic, catalytic and magnetic features of graphene nanocomposites depending on the hybridization along with nanoparticles (NPs) are utilized in numerous applications which includes energy storage, imaging, electronics and catalysis (Kausar et al. 2023; Lee et al. 2022; Sagadevan et al. 2021; Mundal et al. 2023). Previously, considerable efforts are made to combine uniformly different varieties of nanosubstances which include metal oxide and metallic NPs together with graphene that characteristically increase the capabilities of these substances because of the synergistic impact as a consequence of their combination (Ullah et al. 2015; Wang et al. 2014). Besides increasing the capabilities of graphene, NPs also function as a stabilizing agent over the agglomeration of discrete graphene layers, which is prominently caused through the van der Waals attraction between individual graphene sheets (Tang et al. 2014). Additionally, in numerous cases metal NPs intercalation along with graphene assisted in the exfoliation of discrete graphene nanosheets from graphite (Gotoh et al. 2011). Hence, novel approaches and great efforts for fabricating nanohybrids based on graphene are very essential (Kanwal et al. 2021).

Anchoring of metal NPs on the graphene surface for synthesis of nanohybrids is categorized generally by two alternative procedures (Yang et al. 2021): (i) in situ crystallization (in situ attaching) and (ii) ex situ hybridization (post-immobilization). Ex situ hybridization includes blending of discrete solutions of graphene nanolayers and commercially available NPs or prefabricated NPs (Xia et al. 2014). However, in situ crystallization of NPs is performed through concurrent reduction of graphene oxide (GO) and corresponding metallic salts utilizing various reducing agents (Bhirud et al. 2015). Usually, the techniques engaged in NPs in situ crystallization have been extensively utilized because of their low cost as they reduce the number of steps in order to obtain desired product (Leng et al. 2014). Numerous chemical reduction methods are employed during the in situ synthesis of graphene-based nanohybrids, for instance electrochemical, thermal and chemical. Amongst them, chemical method is the widely employed and most hopeful technique for bulk-scale preparation of metallic NPs-graphene nanohybrids (Cobos et al. 2020; Salim et al. 2021). The chemical method stands out as a superior approach for synthesizing graphene-based nanohybrids due to several key advantages like simple and rapid production, easy control of particle size and composition, uniform mixing and large-scale production, making it a preferred choice for synthesizing graphene-based materials with enhanced properties (Majumder et al., 2022).

Numerous nanohybrids have been fabricated through the in situ reduction of various metallic precursors like H_2PdCl_6, K_2PtCl_4, $AgNO_3$, $HAuCl_4$ by employing reducing agents, namely $NaBH_4$, amines and hydrazine hydrate (Han et al. 2013; Zhang et al. 2014a; Xu et al. 2008; Compton et al. 2010). However, nanohybrids synthesized via chemical techniques generally suffered from poor dispersibility and irreversible agglomerations of NPs or/and graphene layers to increase the processing ability of these substances (Dey et al. 2015; Kulia et al. 2012). Additionally, most of the reagents participated in the in situ reduction and functionalization processes of nanohybrids are extremely hazardous by their nature, which are toxic for both human life and environment (Kulia et al. 2013). Furthermore, the existence of these extremely hazardous reductants on the nanohybrids surface in minute quantities could significantly alter capabilities of these substances and have adverse impacts on its application in the field of biology (Yin et al. 2015).

In recent times, trend of employing bioreducing agents in the fabrication of nanosubstances has received immense acceptance (Adil et al. 2015b). For example, different bioreducing agents have been employed for the fabrication of metallic NPs like microbes, bovine serum albumin, glucose, ascorbic acid, amino acids, vitamin C and plant extracts (Hulkoti et al. 2014; Khan et al. 2013a; Bahram et al. 2014; Nadagouda et al. 2007; Hebbalalu et al. 2013). Amongst these bioreducing agents, phyto-extracts have gained considerable interest because of their large-scale amounts, easy availability and low cost (Barman et al. 2013; Akhtar et al. 2013). Additionally, phyto-extracts not only act as a reductant but also serve as a stabilizer, which restrict the application of other chemical capping agents (Makarov et al. 2014; Khan et al. 2014b). Owing to these, phyto-extracts are not utilized only in fabrication of metal NPs; however, in several other cases they are also applied successfully for GO reduction (Khan et al. 2014b). Though several metal NPs are synthesized utilizing phyto-extracts as reductant, their use in the fabrication of nanohybrids based on graphene has been restricted so far (Sedki et al. 2015).

Polyscias scutellaria Fosberg is an indigenous plant extensively employed in traditional medicine to treat a variety of ailments. The antimicrobial properties of P. scutellaria leaves have been investigated, and they are traditionally employed to alleviate body odour, wounds, urinary tract issues and breast inflammation (Rosa et al. 2019). Research has demonstrated that *P. scutellaria* leaves contain bioactive compounds, including alkaloids, saponins, tannins and

flavonoids, and they possess antibacterial properties. The alkaloid is the most bioactive compound in *P. scutellaria*, as it disrupts the stability of peptidoglycan and degrades fungal cell walls. Triterpenoid saponins, another active compound, are renowned for their antifungal properties (Arif et al. 2009). *P. scutellaria* leaves are an appropriate choice as reducing and stabilizing agents due to the presence of these bioactive compounds. On the other hand, Budiono et al. conducted the LC-HRMS to detect bioactive compounds present in aqueous extract of PS extract. Majorly compounds present in PS extract include rutin, quercetin, oleanolic acid, quercetin-3β-D-glucoside, kaempferol and caryophyllene oxide. Further, PS extract also contains five terpenes, seven phenolic and nine flavonoid compounds which including two flavonoid-3-O-glycosides, two flavonoid-7-O-glycosides and seven flavanols (Budiono et al. 2023).

In our present investigation, we have showed fabrication of palladium/highly reduced graphene oxide (RGO/Pd) nanohybrids utilizing *Polyscias scutellaria* leaf extract as bioreducing agent. Several plant biomolecules have been reported for the synthesis of graphene and their nanocomposites (Almas et al. 2014; Fatemeh et al. 2012; Halawany et al. 2012; Alam et al. 2013; Akhtar et al. 2011). In fact, the remarkable reducing capability of *Polyscias scutellaria leaf* extract is utilized for the first time in one of the past investigations for GO reduction (Khan et al. 2015a).

In this study, *Polyscias scutellaria* leaf extract functioned as both in situ functionalization binding agent and reductant, which assisted in anchoring of Pd NPs on the surface of RGO sheets. The fabricated RGO/Pd nanohybrids were analysed by transmission electron microscopy (TEM), Fourier transform infrared (FT-IR) spectroscopy, X-ray photoelectron spectroscopy (XPS), X-ray diffraction (XRD) and ultraviolet-visible (UV/Vis) spectroscopy. Primarily, we observed that the synthesized nanocomposite has the ability to catalyse simultaneous reduction of 2-NA. Furthermore, an added advantage of the as prepared RGO/Pd nanocomposite is its antimicrobial and antifungal ability. Biomolecules present in plant extract are reported to exhibit antimicrobial and antifungal activities which then get adsorbed on the surface of RGO. Pd acts as catalyst exhibiting catalytic activity. Hence, RGO/Pd exhibits potential catalytic and antimicrobial properties. The bactericidal activity of graphene-based metal nanocomposites is significantly influenced by their physicochemical properties (Hu et al. 2010). The combination of palladium nanoparticles and reduced graphene oxide is widely used in the manufacture of medical instruments and apparatus, as it provides exceptional protection against infectious microorganisms (Li et al. 2016; Dou et al. 2015). The outcomes displayed that the nanocomposites exhibited outstanding functioning in the killing of dangerous microbial and fungal pathogens. Further, we exhibited that the mesenchymal stem cells of adult goat were viable in the presence of RGO/Pd of 0.1 mg/mL concentration and their properties of stem cells were retained. All these results strengthen the RGO/Pd composite applicability in future for potential therapy in engineering of bone tissue.

Experimental work

Materials

Graphite powder, Na_2PdCl_4, $NaBH_4$ (98%) and 2-nitroaniline (2-NA, 98%) dye were obtained from Sigma-Aldrich, Shanghai. All the experiments were performed using double-distilled water.

Preparation of Polyscias scutellaria leaf *extract.*

Freshly collected *Polyscias scutellaria* leaves were thoroughly washed utilizing DDW before its application. 10 g of leaves was suspended in 100 mL of deionized (DI) water and boiled on a water bath for approximately 20 min. Then, the mixture was filtered using Whatman No. 1 filter paper to obtain the final filtrate. Later it was brought down to ambient temperature and then stored in a refrigerator condition for future use.

Biofabrication of RGO/Pd NPs utilizing Polyscias scutellaria leaf *extract.*

Graphene oxide (GO) was fabricated from graphite powder utilizing modified hummers technique (Hummak et al. 2021). We followed modified Hummers method for GO synthesis as it exhibits improved level of oxidation, performance of the reaction and reduce the release of toxic gases (Cardoso et al. 2019). Leaf extract was mixed with 100 mg of GO, and this solution was subjected to sonication for about 20 min. Later, the reaction solution was refluxed for approximately 12 h. Reaction mixture colour was transformed to black from light brown owing to surface plasmon resonance (SPR) excitation, which indicates GO reduction. The changes in electronic structure and electronic properties and enhanced electron transfer under SPR conditions lead to changes in absorption or reflection of light, resulting in the colour change. Then the RGO hybrid was separated by performing centrifugation after bringing down to ambient temperature. Then, the obtained residue was rinsed thoroughly using deionized water through successive centrifugation process. In order to suspend well in water, the RGO hybrid was subjected to sonication every time before the process of centrifugation. 20 mL Na_2PdCl_4 of concentration 0.5 M was added drop by drop to 50 mL final aqueous extract, and the resultant mixture was stirred well for 12 h at 100 °C. Lastly, RGO/Pd nanohybrid was sent for centrifugation process to separate from reaction solution, and the final mixture was washed many times utilizing DI water and later air-dried.

Characterization

Using an X-ray powder diffractometer (XRD) with Cu Kα radiation (λ = 0.15406 nm) and a scanning rate of 0.01° per step, the crystal phase of the produced samples was measured. Using Fourier transform infrared (FT-IR) spectroscopy at room temperature in the range of 4000–400 cm^{-1} with an RXI [PerkinElmer], the functional groups of the nanocomposite were examined (Al-Rawi et al. 2020). A Quanta FEG-250 HR-SEM was used to take pictures while a scanning electron microscope (SEM) was used to analyse the composites morphology. A JASCO V-530 spectrophotometer was used to record UV-Vis spectra. An examination was performed utilizing X-ray photoelectron spectroscopy (XPS) with a PHI 5300 apparatus, and a 514-nm laser beam was used to obtain Raman spectra using a micro-Raman spectrometer. Electron-dispersive spectroscopy analysis (EDS) was performed with an electron-dispersive spectroscopy unit (Smjecanin et al. 2022).

Catalytic test

Catalytic ability of produced RGO/Pd nanohybrid was examined utilizing it as catalyst for investigating 2-NA reduction. In conventional methods, reduction procedure for 50 mL aqueous 2-NA solution (0.5 mM) comprising 0.1 g $NaBH_4$ which serves as a reductant, was investigated utilizing 5 mg RGO/Pd nanohybrid as a catalyst. During reaction process, approximately 1 mL sample was removed from the reaction solution at particular time period and placed in quartz cuvette for recording absorption spectrum in a time-based manner. The decrease in the intensity of absorption was observed for nitro compounds at around 410 nm; also, the respective rate constants along with various first concentrations of catalysts are measured. In addition, the reduction process was examined at three different temperatures for studying the influence of temperature and to measure activation energy value for reduction process.

Antimicrobial effect-Agar well diffusion technique

Antimicrobial properties of RGO/Pd nanohybrids were studied utilizing agar well diffusion technique over four different pathogenic fungi like *Tricoderma viride*, *Mucor plumbeus, Candida trophicans* and *Candida albicans*, and 4 pathogenic microbes, namely *Pseudomonas aerunginosa, Bacillus cereus, Bacillus thuringiensis* and *Klebsiella pneumonia,* in Muller-Hilton agar (MHA) media supplemented with standard antibiotic (ketoconazole) suggested by laboratory and clinical standard institute. Cell cultures were washed and placed in petri dishes: approximately 4-mm-diameter-sized wells were punched out in the petri dishes. RGO/Pd nanohybrid was added into each agar well at various doses (50, 30, 20 µL). Dimethyl sulfoxide (DMSO) acts as negative control and the pathogens were cultured in basal medium. At optimal conditions, petri dishes were undergone incubation for about a day at 38 °C. Zone of inhibition diameter was assessed and expressed as mm, optical photographs of petri dishes were recorded, and the nanohybrid which was displaying maximal antibacterial effect for every pathogen was observed and presented in tabular form.

Viability, isolation and adhesion of goat adipose tissue-derived MSCs (AdMSCs) on the LOG NPs

For these studies, the 3D structure of RGO/Pd in bulk form was made for scaffolds, by mixing 4 mg of RGO/Pd to 1X phosphate buffered saline (4 mL). Later, RGO/Pd dispersion (1 mg/mL) was allowed for ultrasonication for about 2 h, which followed by drying at 100 °C. After complete drying of composite, 1X phosphate-buffered saline (100 µL) was added to make into slurry.

MSCs derived from goat adipose tissue used in current study were purchased from TONGWEI Biotechnology Co., Ltd (Shanghai, CN). In vitro evaluation of cell viability and adhesion with MTS analysis (Promega) for 10 days was performed, and by using propidium iodide (PI) dye (Invitrogen) and calcein AM dye (Invitrogen), the properties were confirmed at 7th day through microscope. A 24-well plate coated with RGO/Pd was used to seed Goat Ad MSCs showing the density of 1.0×10^3 cells/well. By following the protocols of manufacturer, the cells were stained and visualized with the help of 40C microscope Zeiss Axiovert (Carl Zeiss), which was equipped with a DS-Qi1Mc Nikon Digital Sight camera. Adipose-derived MSCs were equally seeded onto surfaces of graphene and polystyrene control for comparison as polystyrene plays a role in cellular processes, including proliferation and cell viability.

AdMSCs trilineage differentiation of goat on RGO/Pd

As described previously with the help of media and identical passages we performed adipogenesis, osteogenesis and chondrogenesis on the plates coated with nanoparticles (Khan et al. 2014c). All the assays were performed at the same time on surface of graphene and polystyrene surfaces to compare the results.

Results and discussion

FT-IR spectroscopic analysis was mainly utilized to monitor the surface functionalization procedure and modifications in GO surface chemical compositions throughout the immobilization of phyto-extract, succeeded by anchoring of Pd NPs over it. FT-IR spectrum analogous to RGO/Pd, RGO, GO and *PS* extract is presented in Fig. 1. In the spectrum of leaf extract, absorbency bands centred at 1631, 2947, 3456 cm^{-1} were because of the stretching oscillations correlated with C=O, C−H and phenolic O−H linkages correspondingly. Absorbency peaks appeared at 1095, 1292 and 1434 cm^{-1} were attributed to stretching oscillations of C−N and C=C linkages (Nasrollahzadeh et al. 2016). Generally, FT-IR spectrum of graphene oxide was either diminished or its intensities were considerably decreased after the reduction procedure, which at the same time confirms the fabrication of RGO. Obviously, in FT-IR spectra analogous to RGO/Pd nanocomposite, absorbance bands appeared at ~ 1740 cm^{-1} for the stretching vibrations of C=O linkage and ~ 1630 cm^{-1} for the stretching vibrations of C=C linkage correlated with the disappearance of GO, whereas the intensities of wide band at approximately 3440 cm^{-1} analogous to O−H functionalities are relatively decreased, thus suggesting GO reduction to RGO (Veisi et al. 2019). Absorbance band centred at 3456 cm^{-1} attributed to phenolic O−H functionality was relatively narrow and this phenomenon was due to the O−H peak destruction which occurred because of the consequence of anchoring RGO and Pd NPs on to the surface. Altogether, these results confirm the binding of *PS* extract bioconstituents on the RGO/Pd or RGO surface as a stabilizing agent.

UV-Vis spectroscopic studies were employed to investigate the fabrication of Pd NPs and RGO as well as to confirm the *PS* extract as a reducing agent transforming the GO and Pd^{2+} ions into RGO and Pd NPs correspondingly. UV-Vis spectrum analogous to RGO/Pd nanohybrid, RGO, GO and *PS* extract is presented in Fig. 2. UV spectra representative to *PS* extract (violet) shows the peaks at a wavelength ranging between 210 and 225 nm and 280 and 325 nm which were owing to transition of C=O linkage as well as benzoyl linkage transitions suggesting the existence of phenolics (Nasrollahzadeh et al. 2016). Usually, GO displays 2 different peaks centred at ~ 301 nm attributed to π→π* transitions of C=O linkage and the peak situated at ~ 230 nm was attributed to the π→π* transitions of aromatic C=C linkage. While reducing by PS extract, the plasma peak gradually red-shifts to 270 nm, suggesting that GO is reduced and the electronic conjugation within graphene sheets is restored upon PS extract reduction, reflecting increased π-electron concentration and structural ordering, which is consistent with the restoration of sp2 carbon and possible rearrangement of atoms (Kuila et al. 2011; Chowlla et al. 2010). UV-Vis spectra of biofabricated RGO utilizing *PS* extract displays an extra peak at ~ 230 nm (GO) together with red colour shift to ~ 270 nm (RGO) suggesting the accomplishment of reaction process along with the synthesis of RGO (Veisi et al. 2019). $PdC1_2$ displays a familiar absorbency peak a ~ 420 nm. Without these absorption bands in UV spectra representative to RGO/Pd clearly confirms the instantaneous reduction of both $PdC1_2$ and GO along with the fabrication of RGO/Pd nanocomposite. UV-Vis spectra analogous to RGO/Pd nanocomposite display two absorbency peaks at ~ 325 and ~ 280 nm which were quiet similar to the bands of *PS* extract (Veisi et al. 2016). This

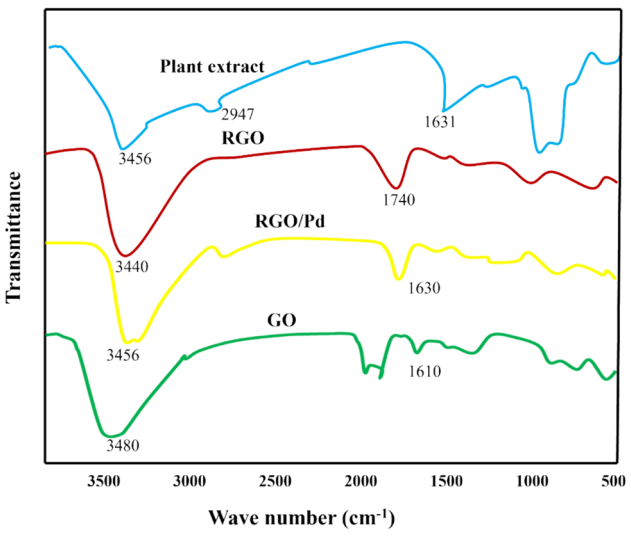

Fig. 1 FT-IR spectrum of plant extract, GO, RGO and RGO/Pd nanocomposite

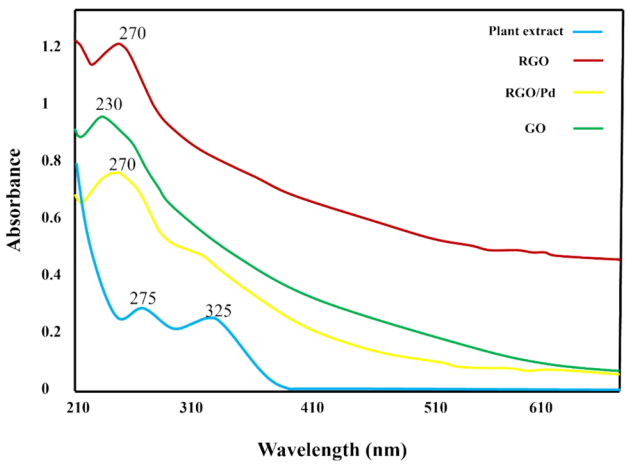

Fig. 2 UV-Vis spectrum of GO, RGO, RGO/Pd and plant extract

evidently shows the presence of leftover plant molecules on RGO/Pd nanohybrid surface as a reductant.

Raman spectroscopy has been considered as an essential method to study the functionalization procedure. Figure 3 displays the Raman spectrum which indicates GO reduction. Two intense absorption peaks of G band (~ 1592 cm^{-1}) and D band (~ 1349 cm^{-1}) were noticed, representative to graphitic (sp^2-hybridized) and diamondoid (sp^3-hybridized) structures, correspondingly. We can observe shift in D and G band in RGO compared to GO, this reflects the reduction process in RGO. This is familiar that D and G band intensity ratio (I_D/I_G) is stringently correlated to with the amount of functionalities. Elevated ratio of I_D/I_G for RGO (i.e. 1.21) over graphene oxide (i.e. 0.89) indicates C=O linkage restoration following the hydrothermal reduction process utilizing leaf extract (Su et al. 2009).

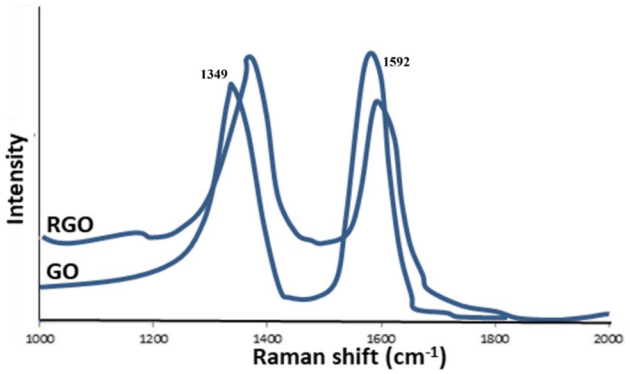

Fig. 3 Raman spectra of GO and RGO. The G band and D band of GO appear at 1592 cm^{-1} and 1349 cm^{-1}

X-ray photoelectron spectroscopy (XPS) was used to evaluate the reduction level and composition of the synthesized RGO/Pd composite. The full-spectrum XPS analysis, as shown in Fig. 4A, indicates the presence of palladium, oxygen, nitrogen and carbon on the surface of the Pd NPs and RGO. The Pd XPS spectra shown in Fig. 4B show two double peaks with binding energies of 340.4 eV and 335.1 eV, respectively, that correspond to $Pd3d_{3/2}$ and $Pd3d_{5/2}$. The fact that these values are in good agreement with the predicted binding energies for metallic Pd indicates that PS extract does not adsorb on the Pd particle surface. The C1s XPS spectra of RGO and GO are shown in Fig. 4C. Only 27% of GO is found in the C1s spectra, but 52% of RGO is attributed to graphitic carbon, which is prominently peaks at 284.6 eV in the RGO spectrum. Compared to 30% in GO, the shoulder peak at 286 eV, which is ascribed to C−OH (epoxy/hydroxy) groups, makes up 19% of the RGO structure. O=C−O, another oxygen-containing group, is present in RGO (288.9 eV) in much smaller amounts than in GO. Furthermore, carbonyl groups are responsible for a new shoulder peak in the RGO profile that is located about 287.6 eV. Figure 4D shows the high-resolution O1s spectra of GO and RGO. The O1s photoelectron peak of GO is located at 532.5 eV, whereas the peak of RGO is located at 532.4 eV. These results suggest that RGO still includes carbonoxygen groups, albeit in smaller amounts.

Using EDS analysis, the new RGO/Pd nanohybrids palladium metal content was confirmed (Fig. 5). The samples weight percentages were 48%, 49% and 3% for carbon, oxygen and palladium, respectively. Palladium has a lower weight proportion than the other elements.

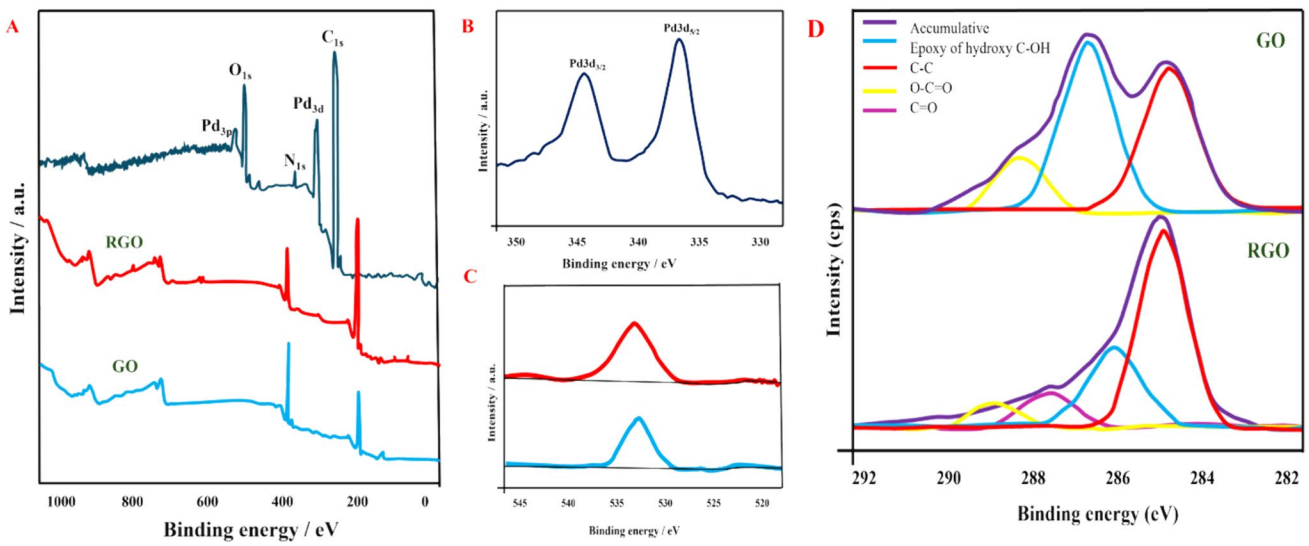

Fig. 4 XPS spectra of RGO/Pd, GO and RGO (**A**), high-resolution Pd spectrum (**B**), high-resolution O1s spectra of RGO and GO (**C**) and high-resolution C1s spectra of RGO and GO (**D**)

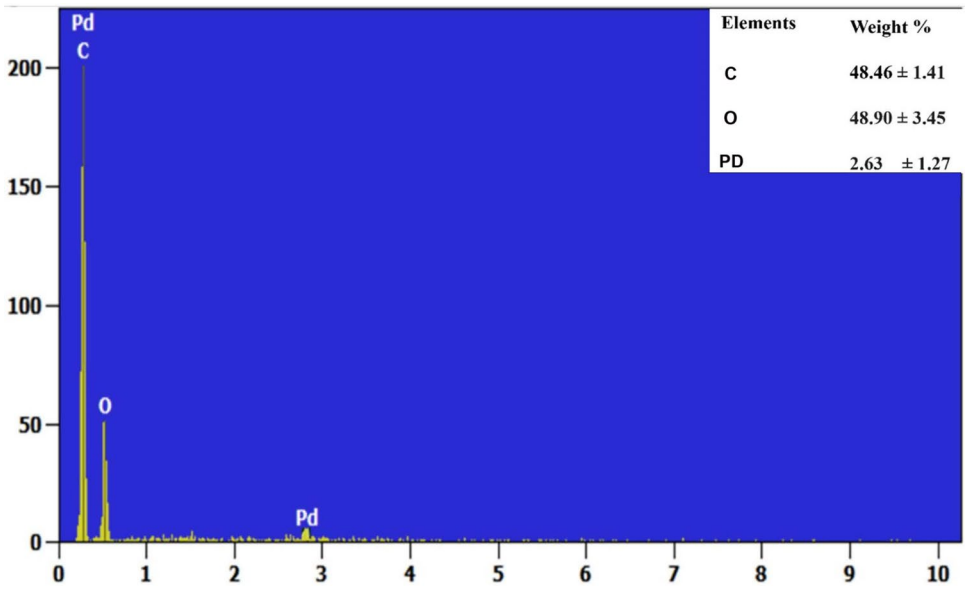

Fig. 5 EDS spectra of RGO/Pd NPs showing the presence of elemental peaks

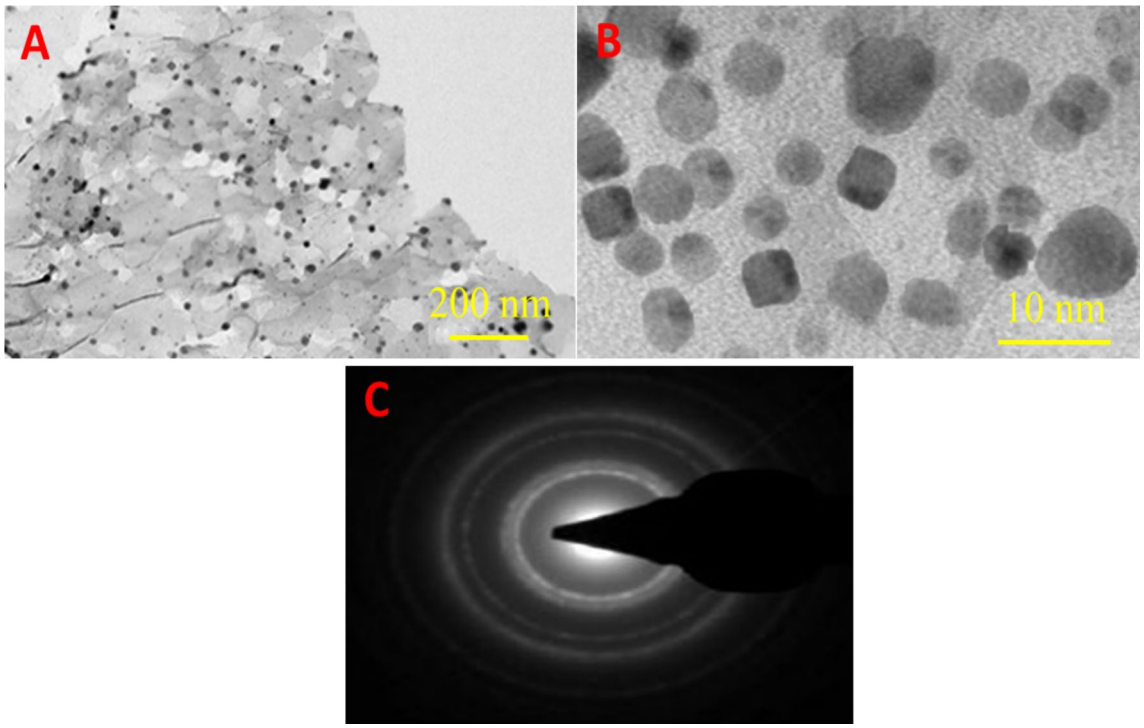

Fig. 6 TEM images (**A**), SAED pattern (**B**) and HR-TEM images (**C**) of RGO/Pd nanocomposite

Mean crystallite size of Pd NPs adhered on the RGO sheet was observed to be 12–15 nm. HR-TEM photographs and SAED pattern of RGO/Pd nanocomposite (Fig. 6) illustrate high crystalline morphology of Pd NPs and the RGO sheet. Inter-planar distance between the fringes was observed to be 0.23 nm which agreed with indexing lattice (111) of Pd face centred cubic (FCC) structure (Chen et al. 2011).

Perfect crystalline morphology and well distribution of Pd NPs over RGO sheets were assigned absolutely to the introduction of bioconstituents exist in extract, which functioned as decorating, stabilizing and reducing agents instantaneously for homogenous immobilization of palladium precursors on the surface of graphene layers with no agglomeration.

Figure 7 displays XRD analysis pattern of synthesized nanohybrid. XRD studies display diffraction peak at 2θ angle value of 10 to 25° at lattice plane (002) correlated with RGO. Sharp peaks centred at 2θ values of 67.7°, 46.4° and 39.9° could be attributed to (220), (200) and (111) indexing planes for the extremely crystalline FCC structure of Pd (Nasrollahzadeh et al. 2016; Veisi et al. 2019).

Catalysis

Fabricated RGO/Pd nanohybrid was investigated for catalytic performance over another environmental contaminant, i.e. reduction of 2-NA other than that specifically for the concurrent reduction of 2-NA and dyes. Reduction of 2-NA was considered as an ideal reaction process to confirm the catalytic capability of fabricated RGO/Pd nanohybrid. Meanwhile, nitro compounds were supposedly very hazardous and these were released as dissipates into water directly from various industries; therefore, their removal or transformation to useful substance is essential (Zhou et al. 2010). Several methods were used for removal of heavy metal ions at trace levels. *Punica granatum* showed effective for preconcentration of seven heavy metal ions (Sulejmanovic et al. 2023). Zahra et al. (2024) used silicate nanoco-polymer for toxic metals extraction. In addition, Ali et.al. (2023) synthesized GO/CuO-NCs and applied for the removal of Ni^{2+} and Cd^{2+} ions from a binary metal ion system. Reduction process was monitored by recording the reduction in absorption near highest peak 410 nm in relation to time. Firstly, reduction reaction was analysed in the existence of $NaBH_4$ alone and noticed that only insignificant proportion of nitro compound had undergone reduction process when compared to amine as depicted in Fig. 8A. The probable causes for this were large energy barrier for activation, and direct reaction between $NaBH_4$ and 2-NA could not produce adequate energy for overcoming that barrier. However, adding appropriate catalyst could accelerate the reduction reaction through a new path which lowers the activation energy.

Hence, 2-NA reduction rate was considerably elevated utilizing RGO/Pd nanohybrid as catalyst which can be noticed by the reduction in 2-NA absorption intensity near 410 nm (Fig. 8B). As this process was performed with large amounts of $NaBH_4$, to predict the values of reduction rate constants pseudo first-order kinetic model was utilized (Ghosh et al. 2004).

Rate equation was given as:

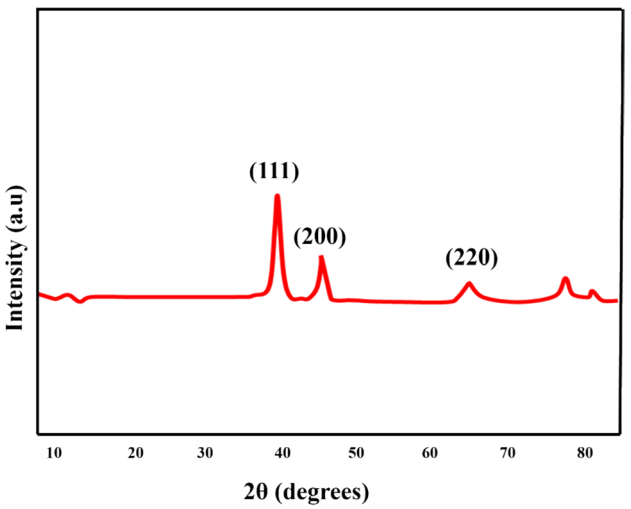

Fig. 7 XRD pattern of RGO/Pd nanocomposite

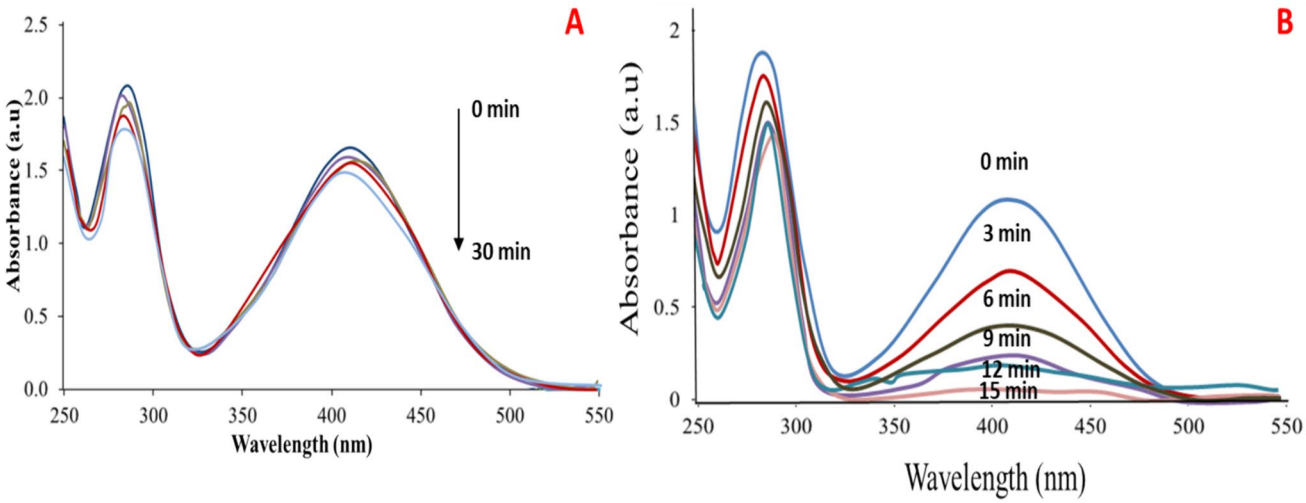

Fig. 8 UV-Vis absorption spectrum showing the gradual reduction of 2-NA **A** without catalyst; **B** with catalyst

$$In\frac{C_t}{C_o} = K_{app.t}$$

where C_o represents initial concentration of 2-NA (mM), C_t represents the concentration at specific time period t and K_{app} was considered as the approximate reduction rate constant. It could be observed by that plotting ln (Ct / Co) over time period gives a straight line for 3 various concentrations of catalytic agent (0.005 g, 0.004 g as well as 0.002 g) (Fig. 9). Elevation in the slope of graphs along with the K_{app} values was noticed with increased catalytic agent concentration from 0.002 g to 0.005 g. Such rise could be described due to the existence of a greater volume of active sites for catalysis that accelerates efficient collisional frequency, and therefore increases rate of catalytic reaction. Hence, quantity of catalytic agent was major tool for checking nitro compound reduction. K_{app} maximal value was observed as 6.48 $\times 10^{-3}$ /sec at 5 mg catalytic agent in this study which is remarkably greater when compared to the values described previously by a researcher (Cheng et al. 2015) for the catalytic reduction of 4-NP utilizing RGO-dependent catalyst. Catalytic performance of Pd NPs-graphene nanohybrid has also been investigated at three various temperatures such as 50, 40 and 30 °C and fixing other factors as constants. Through Fig. 10, it was evident as the linear patterns of ln (Ct / Co) against time period in graphs were noticed at various values of temperature with increased K_{app} value to 7.66 $\times 10^{-3}$ / sec from 3.45 $\times 10^{-3}$ as the temperature raised to 50° from 30 °C. Such an elevation in reduction rate along with temperature raise might be because of greater mean kinetic energies of dye compounds, and therefore increased rate of efficient collisions between the molecules. Steadiness in linear pattern also suggests the uniform scattering of Pd NPs on the surface of RGO sheets (Lin et al. 2011; Ajmal et al. 2014).

Antimicrobial activity

Figures 11, 12, 13 display the antibacterial properties of RGO/Pd nanohybrid, GO over 4 pathogenic bacteria, namely *Pseudomonas aerunginosa, Bacillus cereus, Bacillus thuringiensis* and *Klebsiella pneumonia.* Inhibition zone diameter was assessed after a day. Inhibition zones of various microbes are given in Tab 1. Mechanism of antimicrobial effect of RGO/Pd nanohybrid was dependent on liberation of reactive oxygen species (ROS) (Yamamoto et al. 2000). The chemical reactions amongst hydrogen peroxide (H_2O_2), proteins and additional chemical moieties prevented the microbial growth (Zhang et al. 2008). Microbial plasma membrane composed of proteins, so the Pd NPs exist in the composite disrupt the plasma membrane and react with membrane proteins (Hariharan et al. 2012) which damage and distort the microbial cell. Intra-cellular substances have been leaked; cellular respiratory mechanistic chain was disrupted, resulting in the disorganization and damage to plasma membrane, and finally causes cell death.

Antimicrobial property of fabricated nanohybrid was determined by assessing the inhibition zone diameter over the standard antibiotic amikacin (Figs. 11). Bacteriostatic activity of samples on previously mentioned pathogenic organisms was determined, and maximum inhibitory activity was noticed over gram-positive microbes (*B. cereus* (G+ve) and *B. thuringiensis* (G+ve)). The cell walls of gram-positive microbes composed of peptidoglycan layers can be effortlessly penetrable. Cell walls of gram-negative microbes

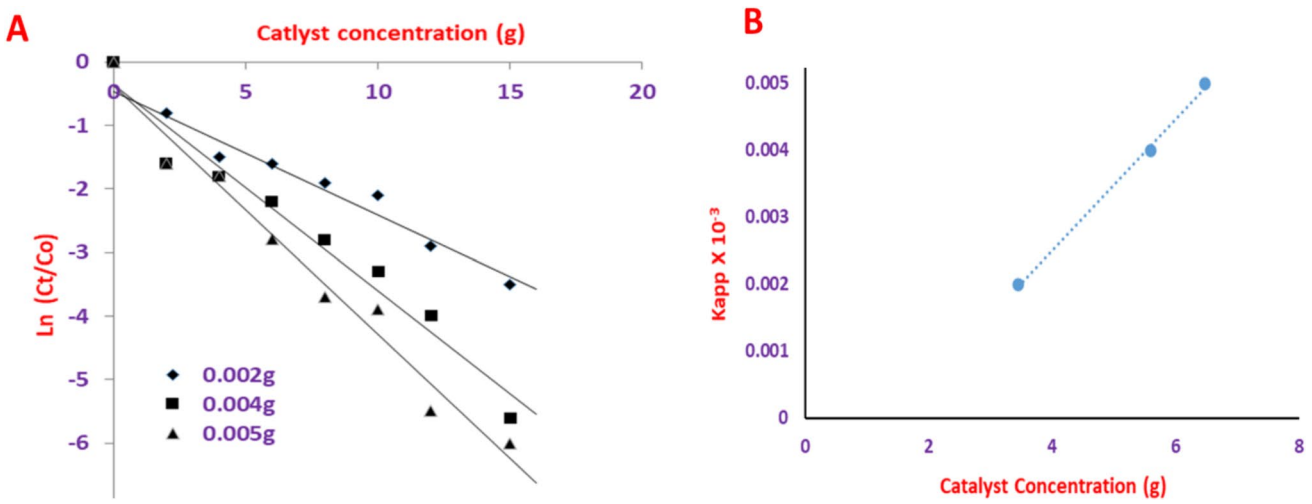

Fig. 9 **A** Effect of RGO/Pd concentration on determination of approximate rate constant (i.e. k_{app}) for 2-NA reduction. (B) k_{app} dependence on the quantity of RGO/Pd catalyst

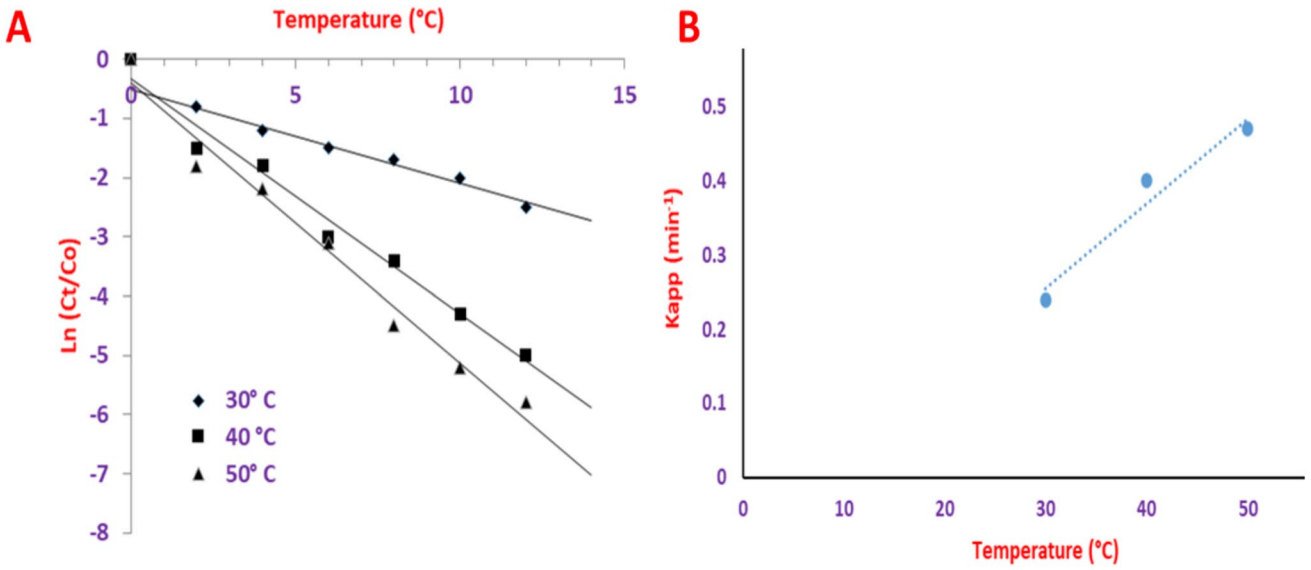

Fig. 10 **A** Effect of temperature on rate constant for 2-NA reduction using RGO/Pd catalyst. **B** k_{app} dependence on temperature

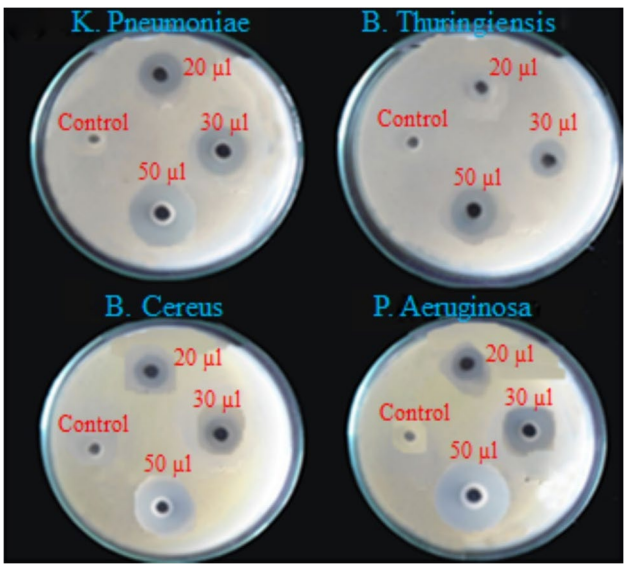

Fig. 11 Antimicrobial activity of RGO/Pd nanocomposite against *K. Pneumoniae*, *B. thuringiensis*, *B. cereus* and *P. aerunginosa*

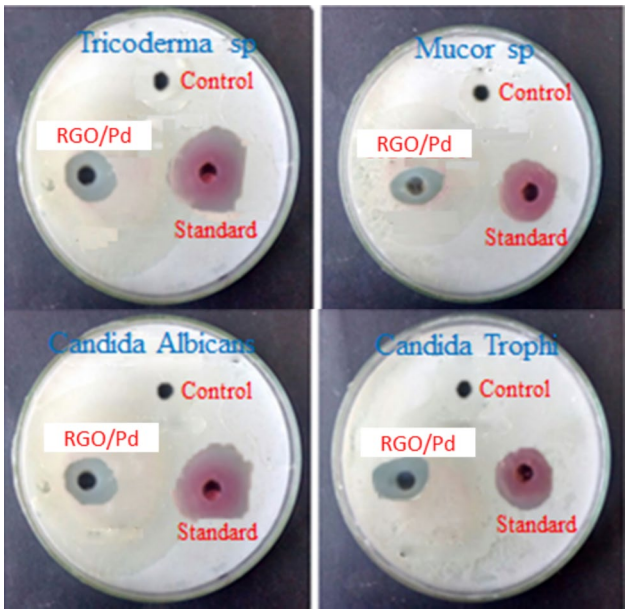

Fig. 12 Antifungal activity of RGO/Pd nanocomposite

were composed of phospholipids along with lipopolysaccharide that renders it as impermeable. Inhibition area of *Bacillus cereus, B. thuringiensis* (G+ve) was 15 as well as 14 mM in diameter correspondingly. Utilized standard antibiotics showed inhibition zone as 17 and 16 mM in diameter for the mentioned microbes. This was because of the existence of Pd NPs adhered on the surface of RGO which was indicated in SEM micrographs. NP shape existing in the complex showed little influence on their activity, greater the surface area of GO, higher the Pd NPs concentration which yields good antimicrobial property (Yamamoto et al. 2003). Electrostatic attraction between negatively charged cellular membrane of pathogens and positively charged NPs increases the antimicrobial capability of RGO/Pd nanohybrid (Dibrov et al. 2002). Similar catalytic and antimicrobial studies were reported by Siddique et al. (2021).

Figure 12 displays the antifungal effect of RGO/Pd nanohybrid over the 4 pathogenic fungi, namely *Tricoderma viride*, *Mucor plumbeus, Candida trophicans* and *Candida albicans*. Evident zone of inhibition was noticed after employing fabricated RGO/Pd nanohybrid over the fungi in

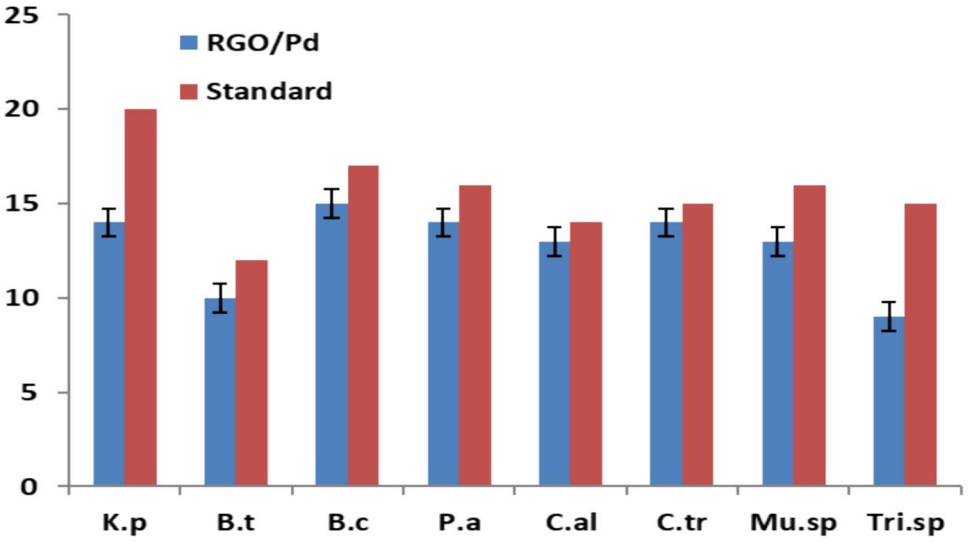

Fig. 13 Antimicrobial and antifungal efficiency histogram of RGO/Pd hybrid over four, mycological and bacterial pathogens

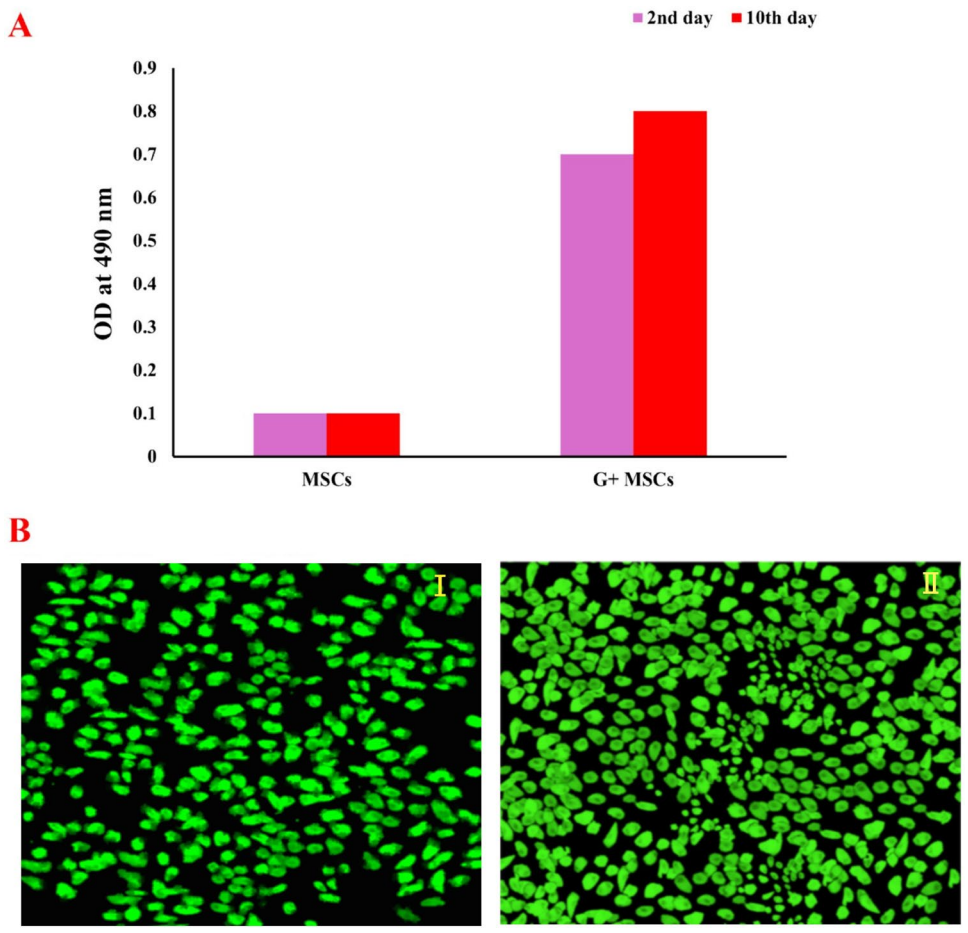

Fig. 14 Cell viability examination by MTT assay (**A**); live-dead fluorescent staining of Control (I) RGO (II) (**B**)

relation to standard antibiotic ketoconazole. Figure 13 displays the antibacterial activity of RGO/Pd nanohybrid over the 4 pathogenic bacteria and fungi along with the standard antibiotics. Similar studies were reported by Selvi et al. (2024).

Biocompatibility studies

MTS proliferation assay was used to evaluate the cell viability of initially isolated and then characterized and cryopreserved goat adipose tissue-derived MSCs in in vitro using

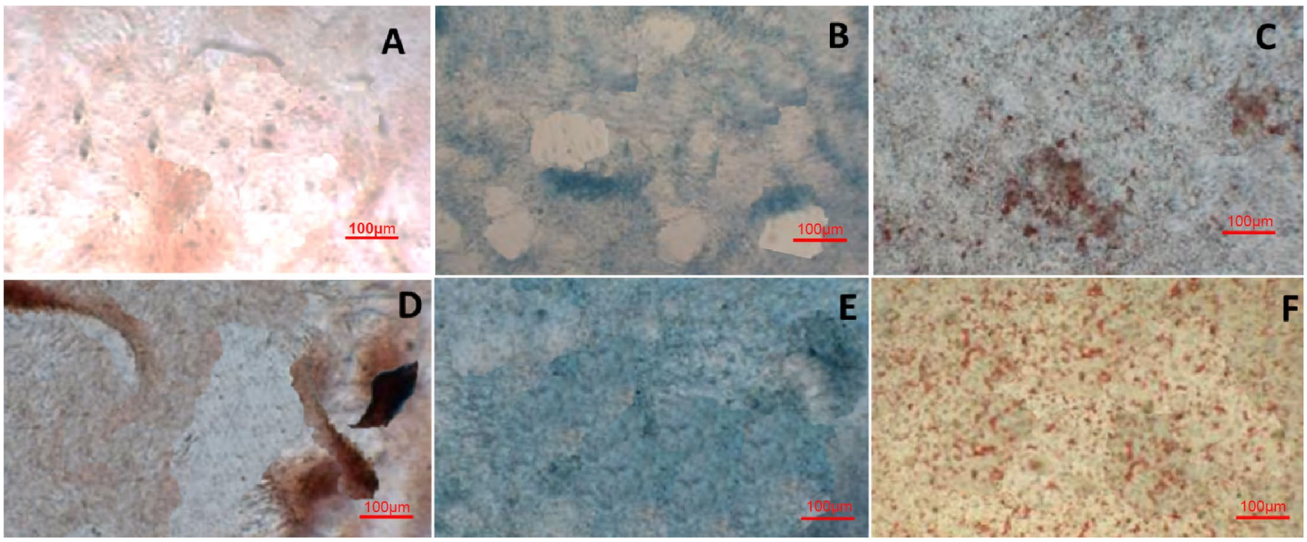

Fig. 15 AdMSCs differentiation was assessed without (**A**-**C**) and with treatment of RGO (**D**-**F**)

RGO films (17). MSCs maintained the cell viability and their proliferation was retained on RGO films, which are similar to the surface coated with polystyrene (Fig. 14A). Later the cell viability was confirmed by fluorescent live-dead staining (Fig. 14B). Using calcein AM dye (green fluorescence), it was concluded that the cells stick to the films of graphene and the cell viability was retained.

Properties of mesenchymal cell in the presence of RGO/Pd

Multipotency of MSCs was determined by trilineage differentiation of mesenchymal stem cells in vitro when RGO is present. As concluded by the staining patterns of oil red o, alizarin red and alcian blue, goat adipose-derived MSCs had undergone adipogenesis, osteogenesis and chondrogenesis, respectively, when media of lineage-specific is present on LOG 2D (Fig. 15).

Conclusions

Environmental-friendly biofabricated palladium nanoparticles adhered to *Polyscias scutellaria* (PS) leaf extract-mediated reduced graphene oxide (RGO/Pd) composite was prepared. The prepared RGO/Pd composite is characterized using different microscopic and spectroscopic techniques. Mean crystallite size of Pd NPs adhered on the RGO sheet was observed to be 12–15 nm. EDS analysis confirmed the presence of Pd, C and O elements in the RGO/Pd nanocomposite. Further, the nanocomposite was tested for their catalytic activity, antifungal, antimicrobial and bone regeneration. The RGO/Pd nanocomposite has shown to be a successful adsorbent for the removal of several industrial dyes from aqueous solutions. It is synthesized using a simple one-step procedure. It also has antimicrobial qualities and acts as an effective catalyst for the elimination of the aromatic pollutant 2-nitroaniline (2-NA). RGO/Pd exhibited very good catalytic efficacy towards the reduction of 2-NA which is an aromatic pollutant. Furthermore, prepared RGO/Pd nanocomposite showed very good antifungal ability. Further, the mesenchymal stem cells of adult goat were viable in the presence of RGO/Pd of 0.1 mg/mL concentration and their properties of stem cells were retained. All these results strengthen the reduced graphene oxide applicability in future for potential therapy in bone tissue engineering applications.

Funding The authors have declared that no funding was associated with this work.

Data availability The data associated with the findings of this study are available from the corresponding authors, upon reasonable request.

Declarations

Conflict of interest All the authors have declared no conflict of interest related to this work.

Ethical statement This research was carried out in line with the principles and standards outlined in the institutional Committee on Ethics of Animal Experimentation. All the animal experiments were performed according to ethical committee guidelines of the First Affiliated Hospital of Guangxi Medical University.

References

Adil SF, Assal M, Khan M, Al-Warthan A, Siddiqui MR, Liz-Marzán LM (2015) Biogenic synthesis of metallic nanoparticles and prospects toward green chemistry. Dalton Trans 44:9709–9717. https://doi.org/10.1039/C4DT03222E

Ajmal M, Siddiq M, Al-Lohedan H, Sahiner N (2014) Highly versatile p (MAc)-M (M: Cu Co, Ni) microgel composite catalyst for individual and simultaneous catalytic reduction of nitro compounds and dyes. RSC Adv 4:59562–59570. https://doi.org/10.1039/C4RA11667D

Akhtar J, Siddique KM, Bi S, Mujeeb M (2011) A review on phytochemical and pharmacological investigations of miswak (Salvadora persica Linn). J Pharm Bioall Sci 3:113–117. https://doi.org/10.4103/0975-7406.76488

Akhtar MS, Panwar J, Yun YS (2013) Biogenic synthesis of metallic nanoparticles by plant extracts. ACS Sustain Chem Eng 1:591–602. https://doi.org/10.1021/sc300118u

Alam MN, Roy N, Mandal D, Begum NA (2013) Green chemistry for nanochemistry: exploring medicinal plants for the biogenic synthesis of metal NPs with fine-tuned properties. RSC Adv 3:11935–11956. https://doi.org/10.1039/C3RA23133J

Ali AH, Kareem AB, Al-Rawi UA, Khalid U, Zhang S, Zafar F, Papraanin E, Hatshan MR, Sher F (2023) Kinetic and equilibrium study of graphene and copper oxides modified nanocomposites for metal ions adsorption from binary metal aqueous solution. Front Chem 11:1279948. https://doi.org/10.3389/fchem.2023.1279948

Almas A, Almas K (2014) Miswak (Salvadora persica chewing stick): the natural toothbrush revisited. Odontostomatol Trop 37:27–39

Al-Rawi UA, Sher F, Hazafa A, Rasheed T, Al-Shara NK, Lima EC, Shanshool J (2020) Catalytic activity of Pt loaded zeolites for hydroisomerization of nhexane using supercritical CO2. Ind Eng Chem Res 59(51):22092–22106. https://doi.org/10.1021/acs.iecr.0c05184

Arif T, Bhosale JD, Kumar N (2009) Natural products-antifungal agents derived from plants. J Asian Nat Prod Res. https://doi.org/10.1080/10286020902942350

Bahram M, Hoseinzadeh F, Farhadi K, Saadat M, Najafi MP, Afkhami A (2014) Synthesis of gold nanoparticles using pH-sensitive hydrogel and its application for colorimetric determination of acetaminophen, ascorbic acid and folic acid. Colloids Surf a: Physicochem Eng Aspects 441:517–524

Ban G, Hou Y, Shen Z, Jia J, Chai L, Ma C (2023) Potential biomedical limitations of graphene nanomaterials. Int J Nanomedicine. 18:1695–1708. https://doi.org/10.2147/IJN.S402954

Barman G, Maiti S, Laha JK (2013) Bio-fabrication of gold nanoparticles using aqueous extract of red tomato and its use as a colorimetric sensor. Nanoscale Res Lett 8:1–9. https://doi.org/10.1186/1556-276X-8-181

Bhirud AP, Sathaye SD, Waichal RP, Ambekar JD, Park CJ, Kale BB (2015) In-situ preparation of N-TiO_2/graphene nanocomposite and its enhanced photocatalytic hydrogen production by H_2S splitting under solar light. Nanoscale 7:5023–5034

Budiono B, Pertami SB, Kasiati Arifah SN, Athoillah MF (2023) Lactogenic effect of Polyscias scutellaria extract to maintain postpartum prolactin and oxytocin in lactating rats. J Ayurveda Integr Med 14(2):100580. https://doi.org/10.1016/j.jaim.2022.100580

Cardoso CED, Almeida JC, Lopes CB, Trindade T, Vale C, Pereira E (2019) Recovery of rare earth elements by carbon-based nanomaterials-a review. Nanomaterials 9(6):814. https://doi.org/10.3390/nano9060814

Chen XM, Wu GH, Chen JM, Chen X, Xie ZX, Wang XR, Am J (2011) A comparative study of CO catalytic oxidation on Pd-anchored graphene oxide and Pd-embedded vacancy graphene. Chem Soc 133:3693–3694. https://doi.org/10.1007/s11051-013-2206-0

Cheng Z, Liao J, He B, Zhang F, Zhang F, Huang X, Zhou L (2015) One-step fabrication of graphene oxide enhanced magnetic composite gel for highly efficient dye adsorption and catalysis. ACS Sustain Chem Eng 3:1677–1685. https://doi.org/10.1021/acssuschemeng.5b00383

Cobos M, De-La-Pinta I, Quindós G, Fernández MJ, Fernández MD (2020) Graphene oxide-silver nanoparticle nanohybrids: synthesis, characterization, and antimicrobial properties. Nanomaterials 10:376. https://doi.org/10.3390/nano10020376

Compton OC, Nguyen ST (2010) Graphene oxide, highly reduced graphene oxide, and graphene: versatile building blocks for carbon based materials. Small 6:711–723. https://doi.org/10.1002/smll.200901934

Dey A, Panja S, Sikder AK, Chattopadhyay S (2015) One pot green synthesis of graphene-iron oxide nanocomposite (GINC): an efficient material for enhancement of thermoelectric performance. RSC Adv 5:10358–10364. https://doi.org/10.1039/C4RA14655G

Dibrov P, Dzioba J, Gosink KK, Hase CC (2002) Chemiosmotic mechanism of antimicrobial activity of Ag + in Vibrio cholera. Chemotherapy 46:2668–2670. https://doi.org/10.1128/aac.46.8.2668-2670.2002

Dou P, Tan F, Wang W, Sarreshteh A, Qiu X, Chen J (2015) One-step microwave assisted synthesis of Ag/ZnO/graphene nanocomposites with enhanced photocatalytic activity. J Photochem Photobiol a: Chem 302:17–22. https://doi.org/10.1016/j.jphotochem.2014.12.012

Fatemeh EA, Mahmoud NS, Hasan F, Farah BK, Mahin A, Zahra H, Hossein D, Mohammad AJ, Hossein B, Faezeh N (2012) Study of the effects of natural toothbrush (Salva-dora persica) in prevention of dental caries and plaque index. Health 4:612–618. https://doi.org/10.4236/health.2012.49096

Fioravanti F, Pérez LA, Chierici JM et al (2023) Synthesis of rGO–Nps hybrids with electrocatalytic activity for hydrogen evolution reaction. J Solid State Electrochem 27:61–74. https://doi.org/10.1007/s10008-022-05304-w

Ghosh SK, Mandal M, Kundu S, Nath S, Pal T (2004) Bimetallic Pt–Ni nanoparticles can catalyze reduction of aromatic nitro compounds by sodium borohydride in aqueous solution. Appl Catal A Gen 268:61–66. https://doi.org/10.1016/j.apcata.2004.03.017

Gotoh K, Kinumoto T, Fujii E, Yamamoto A, Hashimoto H, Ohkubo T, Itadani A, Kuroda Y, Ishida H (2011) Exfoliated graphene sheets decorated with metal/metal oxide nanoparticles:

simple preparation from cation exchanged graphite oxide. Carbon 49:1118–1125. https://doi.org/10.1016/j.carbon.2010.11.017
Halawany HS (2012) A review on miswak (Salvadora persica) and its effect on various aspects of oral health. Saudi Dent J 24:63–69. https://doi.org/10.1016/j.sdentj.2011.12.004
Han TH, Khan MM, Kalathil S, Lee J, Cho MH (2013) Synthesis of positively charged gold nanoparticles using a stainlesssteel mesh. J Nanosci Nanotechnol 13:6140–6144. https://doi.org/10.1166/jnn.2013.7660
Hariharan R, Senthilkumar S, Suganthi A, Rajarajan M (2012) Synthesis and characterization of doxorubicin modified ZnO/PEG nanomaterials and its photodynamic action. J Photochem Photobiol B 116:56–65. https://doi.org/10.1016/j.jphotobiol.2012.08.008
Hashtroudi H et al (2021) Hydrogen gas sensing properties of microwave-assisted 2D Hybrid Pd/rGO: Effect of temperature, humidity and UV illumination. Int J Hydrogen Energy 46:7653–7665. https://doi.org/10.1016/j.ijhydene.2020.11.268
Hebbalalu D, Lalley J, Nadagouda MN, Varma RS (2013) Greener techniques for the synthesis of silver nanoparticles using plant extracts, enzymes, bacteria, biodegradable polymers, and microwaves. ACS Sustain Chem Eng 1:703–712. https://doi.org/10.1021/sc4000362
Hu B, Peng C, Luo WJ, Lv M, Li XM, Li D, Huang Q, Fan CH (2010) Graphene-based antibacterial paper. ACS Nano 4:4317–4320. https://doi.org/10.1021/nn101097v
Hulkoti NI, Taranath T (2014) Biosynthesis of nanoparticles using microbes — a review. Colloids Surf b: Biointerf 121:474–483. https://doi.org/10.1016/j.colsurfb.2014.05.027
Jana A, Scheer E, Polarz S (2017) Synthesis of graphene–transition metal oxide hybrid nanoparticles and their application in various fields. J Nanotechnol 8:688–714. https://doi.org/10.3762/bjnano.8.74
Kanwal A, Yaqoob AA, Siddique A, Bhawani SA, Ibrahim MNM, Umar K (2021) Hybrid Nanocomposites Based on Graphene and Its Derivatives: From Preparation to Applications. In: Qaiss AEK, Bouhfid R, Jawaid M (eds) Graphene and Nanoparticles Hybrid Nanocomposites. Composites Science and Technology
Kausar A et al (2023) Graphene footprints in energy storage systems—an overview. E-Prime-Adv Electr Eng, Electr Energy 6:100361
Khan M, Adil SF, Tahir MN, Tremel W, Alkhathlan HZ, Al-Warthan A, Siddiqui MRH (2013) Green synthesis of silver nanoparticles mediated by Pulicaria glutinosa extract. Int J Nanomed 8:1507–1516. https://doi.org/10.2147/ijn.s43309
Khan M, Kuniyil M, Adil SF, Al-Warthan A, Alkhathlan HZ, Tremel W, Tahir NM, Siddiqui MRH (2014) Biogenic synthesis of palladium nanoparticles using Pulicaria glutinosa extract and their catalytic activity towards the Suzuki coupling reaction. Dalton Trans 43:9026–9031. https://doi.org/10.1039/c3dt53554a
Khan M, Al-Marri AH, Shaik MR, Mohri N et al (2015) Green approach for the effective reduction of graphene oxide using Salvadora persica L root (miswak) extract. Nanoscale Res Lett 10:281. https://doi.org/10.1186/s11671-015-0987-z
Kuila T, Bose S, Khanra P, Mishra AK, Kim NH, Lee JH (2011) Recent advances in graphene-based biosensors. Biosens Bioelectr 26:4637–4648. https://doi.org/10.1016/j.bios.2011.05.039
Kuila T, Bose S, Mishra AK, Khanra P, Kim NH, Lee JH (2012) Chemical functionalization of graphene and its applications. Prog Mater Sci 57:1061–1105. https://doi.org/10.1016/j.pmatsci.2012.03.002
Kuila T, Mishra AK, Khanra P, Kim NH, Lee JH (2013) Recent advances in the efficient reduction of graphene oxide and its application as energy storage electrode materials. Nanoscale 5:52–71. https://doi.org/10.1039/C2NR32703A
Lee SY, Kwon M, Raja IS, Molkenova A, Han DW, Kim KS (2022) Graphene-Based Nanomaterials for Biomedical Imaging. In: Han DW, Hong SW (eds) Multifaceted Biomedical Applications of Graphene. Advances in Experimental Medicine and Biology
Leng J, Wang WM, Lu LM, Bai L, Qiu XL (2014) DNAtemplated synthesis of PtAu bimetallic nanoparticle/graphene nanocomposites and their application in glucose biosensor. Nanoscale Res Lett 9(99):1–8. https://doi.org/10.1186/1556-276X-9-99
Li W, Wang F, Liu Y, Wang J, Yang J, Zhang L, Elzatahry A, Al-Dahyan D, Xia Y, Zhao D (2015) General strategy to synthesize uniform mesoporous TiO2/graphene/mesoporous TiO2 sandwich-like nanosheets for highly reversible lithium storage. Nano Lett 15(3):2186—2193. https://doi.org/10.1021/acs.nanolett.5b00291
Li R, Mansukhani ND, Guiney LM, Ji Z, Zhao Y, Chang CH, French CT, Miller JF, Hersam MC, Nel AE, Xia T (2016) Identification and optimization of carbon radicals on hydrated graphene oxide for ubiquitous antibacterial coatings. ACS Nano 10:10966–10980. https://doi.org/10.1021/acsnano.6b05692
Lin FH, Doong RA (2011) Bifunctional Au– Fe3O4 heterostructures for magnetically recyclable catalysis of nitrophenol reduction. J Phys Chem C 115:6591–6598. https://doi.org/10.1021/jp110956k
Majumder P, Gangopadhyay R (2022) Evolution of graphene oxide (GO)-based nanohybrid materials with diverse compositions: an overview. RSC Adv 12(9):5686–5719. https://doi.org/10.1039/d1ra06731a
Makarov VV, Makarova SS, Love AJ, Sinitsyna OV, Dudnik AO, Yaminsky IV, Taliansky ME, Kalinina NO (2014) Biosynthesis of stable iron oxide nanoparticles in aqueous extracts of Hordeum vulgare and Rumex acetosa plants. Langmuir 30:5982–5988. https://doi.org/10.1021/la5011924
Nadagouda MN, Varma RS (2007) A greener synthesis of core (Fe, Cu) -shell (Au, Pt, Pd, and Ag) nanocrystals using aqueous vitamin C. Cryst Growth Des 7:2582–2587
Nasrollahzadeh M, Sajadi SM, Rostami VA, Alizadeh M, Bagherzadeh M (2016) Green synthesis of CuO nanoparticles using aqueous extract of Thymus vulgaris L. leaves and their catalytic performance for N-arylation of indoles and amines. J Colloid Interface Sci 466:360–368. https://doi.org/10.1016/j.jcis.2015.12.018
Parnianchi F, Nazari M, Maleki J et al (2018) Combination of graphene and graphene oxide with metal and metal oxide nanoparticles in fabrication of electrochemical enzymatic biosensors. Int Nano Lett 8:229–239. https://doi.org/10.1007/s40089-018-0253-3
Radulescu D, Surdu M, Ficai VA, Ficai A, Grumezescu D, Andronescu AM (2023) Green synthesis of metal and metal oxide nanoparticles: a review of the principles and biomedical applications. Int J Mol Sci 24:15397. https://doi.org/10.3390/ijms242015397
Rasuli H, Rasuli R (2023) Nanoparticle-decorated graphene/graphene oxide: synthesis, properties and applications. J Mater Sci 58:2971–2992. https://doi.org/10.1007/s10853-023-08183-2
Rosa D, Halim Y, Kam N, Sugata M, Samantha A (2019) Antibacterial activity of polyscias scutellaria fosberg against acenobacter SP. Asian J Pharm Clin Res. https://doi.org/10.22159/ajpcr.2018.v12i1.30270
Sagadevan S, Shahid MM, Yiqiang Z, Oh W-C, Soga T, Anita L, Jayasingh A, Solhe F, Fatimah I, Waqar A, Paiman S, Johan MR (2021) Functionalized graphene-based nanocomposites for smart optoelectronic applications. Nanotechnol Rev 10(1):605–635. https://doi.org/10.1515/ntrev-2021-0043
Salim MH et al (2021) Characterization Techniques for Hybrid Nanocomposites Based on Graphene and Nanoparticles. In: Bouhfid R, Jawaid M (eds) Qaiss AEK. Graphene and Nanoparticles Hybrid Nanocomposites. Composites Science and Technology. Springer, Singapore
Scroccarello A, Álvarez-Diduk R, Della Pelle F, de Carvalho CE, Silva C, Idili A, Parolo C, Compagnone D, Merkoçi A (2023) One-step laser nano structuration of reduced graphene oxide films embedding metal nanoparticles for sensing applications. ACS Sens 8(2):598–609. https://doi.org/10.1021/acssensors.2c01782
Sedki M, Mohamed MB, Fawzy M, Abdelrehim DA, AbdelMottaleb MM (2015) Phytosynthesis of silver–reduced graphene oxide (Ag–RGO)

nanocomposite with an enhanced antibacterial effect using Potamogeton pectinatus extract. RSC Adv 5:17358–17365. https://doi.org/10.1039/C4RA13117G

Selvi MSG, Jauhar RM, Sivaraj D et al (2024) Enhanced antifungal properties of the Ag-decorated GO and rGO nanocomposites for medical applications. Bull Mater Sci 47:27. https://doi.org/10.1007/s12034-023-03106-y

Siddique S, Zain-ul A, Waseem M et al (2021) Photo-catalytic and antimicrobial activities of rGO/CuO nanocomposite. J Inorg Organomet Polym 31:1359–1372. https://doi.org/10.1007/s10904-020-01760-x

Smjecanin N, Nuhanovi M, Sulejmanovi J, Grahek, Odobai A (2022) Study of uranium biosorption process in aqueous solution by red beet peel. J Radioanal Nucl Chem 331(3):1459–1471. https://doi.org/10.1007/s10967-022-08192-6

Su CY, Xu Y, Zhang W, Zhao J, Tang X, Tsai CH, Li LJ (2009) Electrical and Spectroscopic Characterizations of Ultra-Large Reduced Graphene Oxide Monolayers Chem. Mater 21:5674–5680. https://doi.org/10.1021/cm902182y

Sulejmanovi J, Skopak E, ehovi E, Karada A, Zahirovi A, Smjeanin N, Mahmutovi O, Ansar S, Sher F (2023) Surface engineered functional biomaterials for hazardous pollutants removal from aqueous environment. Chemosphere 336:139205. https://doi.org/10.1016/j.chemosphere.2023.139205

Tang M, Wang X, Wu F, Liu Y, Zhang S, Pang X, Li X, Qiu H (2014) Au nanoparticle/graphene oxide hybrids as stabilizers for Pickering emulsions and Au nanoparticle/graphene oxide@polystyrene microspheres. Carbon 71:238–248

Ullah K, Ye S, Lei Z, Cho K, Oh Y (2015) Synergistic effect of $PtSe_2$ and graphene sheets supported by TiO_2 as cocatalysts synthesized via microwave techniques for improved photocatalytic activity. Cat Sci Technol 5:184–198. https://doi.org/10.1039/C4CY00886C

Veisi H, Rashtiani A, Barjasteh V (2016) Biosynthesis of palladium nanoparticles using *Rosa canina* fruit extract and their use as a heterogeneous and recyclable catalyst for Suzuki-Miyaura coupling reactions in waterAppl. Organometal Chem 30:231–235. https://doi.org/10.1002/aoc.3421

Veisi H, Ghorbani M, Hemmati S (2019) Sonochemical in situ immobilization of Pd nanoparticles on green tea extract coated Fe3O4 nanoparticles: an efficient and magnetically recyclable nanocatalyst for synthesis of biphenyl compounds under ultrasound irradiations. Mat Sci Eng C 98:584–593. https://doi.org/10.1016/j.msec.2019.01.009

Wang Y, Polavarapu L, Liz-Marza N (2014) Reduced graphene oxide-supported gold nanostars for improved SERS sensing and drug delivery. ACS Appl Mater Interf 6:21798–21805. https://doi.org/10.1021/am501382y

Xu C, Wang X, Zhu J (2008) Graphene–metal particle nanocomposites. J Phys Chem C 112:19841–19845. https://doi.org/10.1021/jp807989b

Yamamoto O, Sawai J, Sasamoto T (2000) Change in antibacterial characteristics with doping amount of ZnO in MgO–ZnO solid solution. J Inorg Mater 2:451–454. https://doi.org/10.1016/S1466-6049(00)00045-3

Yamamoto O, Hotta M, Sawai J, Sasamoto T, Kojima H (2003) Antifungal characteristics of spherical carbon materials with zinc oxide. J Ceram Soc Jpn 111(8):614–616. https://doi.org/10.2109/jcersj.111.614

Yang W et al (2021) Graphene oxide-based noble-metal nanoparticles composites for environmental application. Compos Commun 24:100645. https://doi.org/10.1016/j.coco.2021.100645

Yin PT, Shah S, Chhowalla M, Lee KB (2015) Design, synthesis, and characterization of graphene-nanoparticle hybrid materials for bioapplications. Chem Rev 115:2483–2531. https://doi.org/10.1021/cr500537t

Zhang L, Ding Y, Povey M, York D (2008) ZnO nanofluids: a potential antibacterial agent. Prog Nat Sci 18:939–944. https://doi.org/10.1016/j.pnsc.2008.01.026

Zhang C, Zhu X, Wang Z, Sun P, Ren Y, Zhu J, Xiao D (2014) Facile synthesis and strongly microstructure-dependent electrochemical properties of graphene/manganese dioxide composites for supercapacitors. Nanoscale Res Lett 9(490):1–8. https://doi.org/10.1186/1556-276X-9-490

Zhou L, Gao C, Xu W (2010) Robust Fe3O4/SiO2-Pt/Au/Pd magnetic nanocatalysts with multifunctional hyperbranched polyglycerol amplifiers. Langmuir 26:11217–11225. https://doi.org/10.1021/la100556p